^{4}He$(p,2p)^3$H reaction at intermediate energies

W. T. H. van Oers, B. T. Murdoch,* B. K. S. Koene,†
D. K. Hasell, and R. Abegg‡
Department of Physics, University of Manitoba, Winnipeg, Manitoba R3T 2N2, Canada

D. J. Margaziotis and M. B. Epstein
Department of Physics, California State University, Los Angeles, California 90032

G. A. Moss, L. G. Greeniaus, J. M. Greben, and J. M. Cameron
Nuclear Research Center, University of Alberta, Edmonton, Alberta T6G 2J1, Canada

J. G. Rogers
TRIUMF, Vancouver, British Columbia V6T 2A3, Canada

A. W. Stetz
Department of Physics, Oregon State University, Corvallis, Oregon 97331
(Received 5 June 1981)

The ^{4}He$(p,2p)^3$H reaction has been studied at 250, 350, and 500 MeV using coplanar symmetric and asymmetric geometries. The data are presented as energy-sharing spectra, coplanar symmetric angular distributions, and quasifree angular distributions. A comparison with distorted wave impulse approximation calculations indicates reasonable agreement for small recoil momenta ($q \lesssim 150$ MeV/c). For larger recoil momenta, the distorted-wave impulse approximation calculations increasingly underestimate the data. The discrepancies are substantially reduced by inclusion of a spin-orbit term in the optical potential used to generate the distorted waves. Improvements of the single particle wave function for the struck nucleon influence the calculations to a lesser degree. The remaining discrepancies at large recoil momenta may, in part, be ascribed to multiple scattering effects and exchange processes not included in the standard distorted-wave impulse approximation.

[NUCLEAR REACTIONS ^{4}He$(p,2p)^3$H; measured $d^3\sigma/(d\Omega_3 d\Omega_1 dT_3)$, 250, 350, 500 MeV, energy sharing spectra, coplanar symmetric angular distributions, quasifree angular distributions; comparison with DWIA calculations.]

I. INTRODUCTION

Studies of $(p,2p)$ quasifree scattering from the very light nuclei have been concerned largely with the extraction of single-particle wave functions in the framework of the distorted-wave impulse approximation (DWIA). Such studies of ^{4}He$(p,2p)^3$H have been made at 65, 85, and 100 MeV,[1] at 156 MeV,[2] at 460 MeV,[3] and at 590 MeV.[4] All experiments have been performed using coplanar symmetric geometries. Whereas at 590 MeV there is a good agreement between the data near zero recoil momentum and DWIA calculations, agreement between the zero-recoil momentum data at the lower energies and the DWIA calculations could only be obtained after the latter had been renormalized by a factor of $\sim$0.5. Below incident proton energies of 100 MeV or so, one questions the validity of the DWIA but obviously there exists a discrepancy between the results at

460 and 590 MeV (see Fig. 4). At 590 MeV the differential cross section data or the extracted single particle momentum distribution agree with the DWIA calculations up to recoil momenta of ~ 200 MeV/c. For larger recoil momenta the DWIA prediction increasingly underestimates the data for increasing recoil momenta.

The motivation of the present experiment were to resolve the existing ambiguity between the 460 and 590 MeV data, but more fundamentally to test the applicability of the DWIA for the ^{4}He$(p,2p)^3$H reaction by extending the measured region of the single particle momentum distribution in ^{4}He to 500 MeV/c.

In the plane-wave impulse approximation (PWIA), the differential cross section can be expressed in factorized form (reflecting the first order diagram given in Fig. 1):

$$d^3\sigma/(d\Omega_3 d\Omega_4 dT_3) = F(d\sigma/d\Omega)^{\vec{p}_1\vec{p}_2}_{pp} N_p \times |\phi(\vec{q}=-\vec{p}_5)|^2 ,$$

where F is the kinematic factor,

$$F=\frac{(E'_{pp})^2}{p_1}\frac{p_3 {p_4}^2}{E_4p_4+E_5p_4+E_4p_3\cos(\theta_3+\theta_4)-E_4p_1\cos\theta_4}\frac{m_5}{m_1} ,$$

with E'_{pp} the center of mass (c.m.) energy of the two interacting protons. $(d\sigma/d\Omega)^{\vec{p}_1\vec{p}_2}_{pp}$ is the half-off-the-energy-shell proton-proton differential cross section, N_p is the spectroscopic factor [2 in the case of ^{4}He$(p,2p)^3$H], and $\phi(\vec{q}=-\vec{p}_5)$ is the Fourier transform of the overlap integral between the recoiling nucleus (^{3}H) and the target nucleus (^{4}He):

$$\phi(\vec{q}=-\vec{p}_5)=\frac{1}{(2\pi)^{3/2}}\int \exp(i\vec{q}\cdot\vec{r}) \times \langle \psi_{^3\mathrm{H}}/\psi_{^4\mathrm{He}} \rangle d\vec{r} .$$

The obvious refinement is to take into account distortion effects between the incident proton and the core nucleus in the initial state and between the scattered and ejected protons and the core nucleus in the final state. In this case the single particle momentum distribution $\phi(\vec{q}=-\vec{p}_5)$ becomes the distorted momentum distribution

$$\phi(\vec{q})=\int \chi_3^{(-)*}(\vec{r})\chi_4^{(-)*}(\vec{r})\phi(\vec{r})\chi_1^{(+)}(\alpha\vec{r})d\vec{r} ,$$

where the various χ's represent the distorted waves and $\alpha=\frac{3}{4}$.

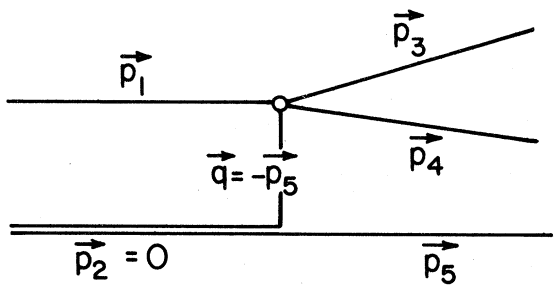

FIG. 1. First order diagram for the quasifree scattering process ^{4}He$(p,2p)^3$H. Here particle 1 represents the incident proton, 2 the target nucleus, 3 the scattered proton, 4 the ejected proton, and 5 the core nucleus which recoils with the momentum it had before the interaction took place.

As described in detail by Roos,[5] there are three types of quasifree scattering experiments most commonly performed:

(1) *The measurement of the energy-sharing spectra.* Here, one selects the coplanar symmetric angle pair ($\theta_3=\theta_4$, $\phi_{3,4}=\pi$) for which the kinematically allowed locus of events in the T_3-T_4 plane contains the point corresponding to zero recoil momentum of the core nucleus. Since for this geometry the p-p differential cross section does not vary greatly in energy and angle, the measured energy distribution or its projection on one of the energy axes (let us say T_3) reflects primarily the distorted momentum distribution.

(2) *The measurement of the coplanar symmetric angular distributions.* Here, one selects a series of coplanar symmetric angles ($\theta_3=\theta_4$, $\theta_{3,4}=\pi$) and extracts from the measured energy distributions the cross section at $T_3=T_4$. The recoil momentum of the core will be either parallel or antiparallel to the incident beam direction depending on whether the opening angle $\theta_3+\theta_4$ is greater than or smaller than the opening angle for the energy sharing spectrum at the same incident energy. The p-p differential cross sections have to be evaluated at c.m. energies which may vary appreciably and at c.m. scattering angles which are always 90°. The extracted $(p,2p)$ cross sections as functions of angle ($\theta_3=\theta_4$) or of recoil momentum will reflect both

the varying two-body cross section and the distorted momentum distribution.

(3) *The measurement of the quasifree angular distributions.* Here, one varies the coplanar angle pair (θ_3,θ_4, $\phi_{3,4}=\pi$); however, θ_3 and θ_4 are chosen in such a way that the locus of kinematically allowed events in the T_3-T_4 plane contains a point for which the recoil momentum of the core nucleus is zero. Assuming distortion effects not to be too angular and energy dependent, the ratio $(d^3\sigma/d\Omega_3 d\Omega_4 dT_3)_{\vec{p}_5=0}/FN_p$ should be proportional to the p-p cross section and is thus a test of the factorization approximation. For the latter type of measurements, additional information may follow from the determination of the asymmetry in $(d^3\sigma/d\Omega_3 d\Omega_4 dT_3)_{\vec{p}_5=0}$ using incident polarized proton beams. It is to be noted that factorization of cross sections is a valid concept only if spin-orbit effects can be neglected.

In the present experiment, a study has been made of the ^{4}He$(p,2p)^3$H reaction at 250, 350, and 500 MeV using the three types of measurements defined above. In the next section, a short description is presented of the experiment; Sec. III presents the data reduction; Sec. IV presents the results and a comparison with previous results; Sec. V describes the DWIA calculations and the input to these calculations; while Sec. VI contains a discussion and some conclusions. A first account of this work was presented recently in the form of a Letter.[6]

II. EXPERIMENT

The experiment was performed using the variable energy proton beam from the TRIUMF accelerator. Proton beams of 250, 350, and 500 MeV, respectively, bombarded a liquid helium target. Beam intensities ranged between 0.2 and 10 nA. The beam spot size and its position were monitored regularly by viewing a scintillator which could be placed at the target position. The cross section of the beam at the target was approximately 1 by 1.5 cm (width and height). The liquid helium target had a thickness of 97 mg cm^{-2} with an aperture of 5.1 by 5.1 cm.[7] The target cell could be raised and lowered remotely. This permitted the liquid helium target cell to be replaced with a dummy cell in order to allow appropriate background subtractions. The target cell could also be rotated around a central vertical axis in order to ensure that the reaction products would not strike the side frames of the target cell.

The scattered and ejected protons were detected in coincidence by two pairs of range telescopes mounted on four independently movable booms which could be positioned remotely about the target axis to an accuracy of 0.1°. Each range telescope consisted of two 0.6 cm thick plastic scintillator detectors, a set of vertical and horizontal multiwire proportional chambers, an appropriate amount of copper absorber, and a 7.6 cm thick by 12.7 cm diameter NaI(Tl) detector (see Fig. 2). The first plastic scintillator, used only in the latter part of the measurements, was positioned as close as possible to the 70 cm diameter scattering chamber enclosing the l^{4}He cryostat tail section. This scintillator served to reduce the number of unwanted coincidence events by restricting the field of view of the range telescopes. The second plastic scintillator provided the trigger signal corresponding to coincident events. The 12.7 by 12.7 cm multiwire proportional chambers were located at distance varying between 1.3 and 2.0 m from the target center. Owing to the limited range for protons of the range telescopes, the energy sharing spectra were measured in a series of overlapping energy bites achieved by placing different amounts of copper absorber in front of the stopping counters. For each measurement, a separate determination was made of the background by replacing the l^{4}He target cell with the empty dummy cell. Energy calibration data were taken at each run using a CH_2 target.

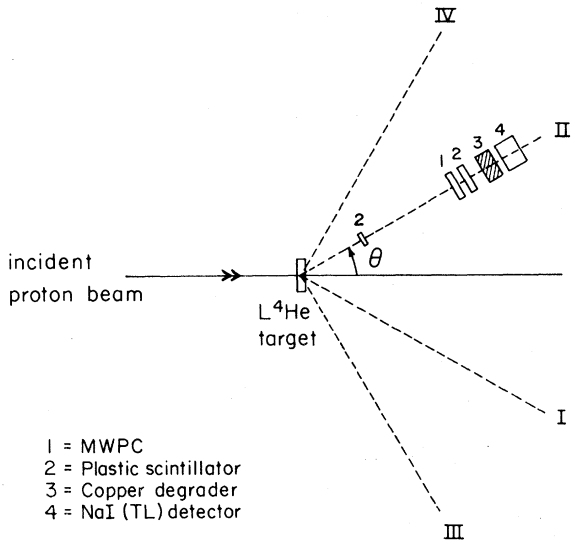

FIG. 2. Schematic diagram of the experimental arrangement.

The absolute scale of the measurements was obtained from a polarimeter placed 3.2 m upstream from the target center. The total incident beam was determined from the sum of left plus right proton-proton events scattered by the ~ 5 mg cm^{-2} thick, CH_2 target of the polarimeter. An independent determination of the absolute scale of the measurements was obtained by integrating the current of an ionization chamber placed 3.0 m downstream from the target center. The ionization chamber and polarimeter had been calibrated previously against a Faraday cup installed in the beam line. The consistency of the absolute normalization of data taken in different experimental runs was checked by repeating, each time, the measurement of the energy bite containing the zero-recoil momentum point of the 500 MeV energy sharing spectrum at 40°—40°.

III. DATA REDUCTION

Data stored on magnetic tape were analyzed using, for the most part, the program KIOWA. This analysis utilized the IBM 360-91 and 3033 computers at UCLA, the PDP 11/34 minicomputer at California State University, Los Angeles, and the Amdahl 470/V7 computer at the University of Manitoba.

Among its various functions, the KIOWA code converted the analog-to-digital converter (ADC) channel to energy, calculated the binding (or missing) energy for each event from the energies and angles of the outgoing protons, and produced histograms and two-parameter plots subject to various conditions. For example, events were rejected if a hit was not recorded on both planes of the wire chamber of each range telescope, or if hits were recorded on nonadjacent wires on a single plane. Acceptable events were confined to those incident within the flat efficiency response region of the NaI(Tl) detectors (less than 5 cm radius from the center of the detector). Real coincidences were separated from accidental coincidences and events belonging to the kinematic locus of the ^{4}He$(p,2p)^3$H reaction were identified by an appropriate cut on the missing mass spectrum. The projections of the two-parameter spectra that satisfied all the above requirements were further corrected for wire chamber inefficiencies corresponding to missing or nonadjacent hits, for NaI(Tl) detector inefficiencies, and for dead time of the overall data acquisition system. The NaI(Tl) detector efficiencies had been determined in a previous measurement.[8] The dead time correction was determined by the ratio of pulses received by the computer versus those sent simultaneously to light-emitting diodes (LED's) attached to each plastic and NaI(Tl) counter as well as to each wire chamber. Final experimental fivefold differential cross sections were obtained following normalization for incident beam current, target thickness, solid angles, and subtraction of accidentals and background. Background information obtained from the target-out measurements had been processed in an identical manner as the target-in measurements. In the case of the energy spectra of the asymmetric pairs of angles taken at 250 and 500 MeV and shown in Fig. 7, the cross sections shown are the weighted average of the values obtained with the unpolarized proton beam and the values obtained with the polarized beam by averaging over spin up and spin down.

IV. RESULTS

The measured energy sharing spectra at 250, 350, and 500 MeV are shown in Fig. 3. The abscissae give both the energy (T_3) of one of the observed protons and the recoil momentum ($\vec{q}=-\vec{p}_5$) of the core nucleus. The uncertainty in the absolute normalization of the differential cross sections is estimated to be 10%. It includes contributions from the uncertainties in the determination of the total number of incident protons, counter and wire chamber efficiencies, solid angles, target thickness, and computer dead time. The energy resolution was such that missing mass spectra showed resolutions varying between 4% and 9% (FWHM) depending on incident energy and experimental run. From these spectra, the estimated contribution of triton breakup events to the cross sections shown is less than 20% in the region of $p_5 \geq 400$ MeV/c and less than 7% at $p_5=0$ MeV/c. Since a pair of integer angles ($\theta_3=\theta_4=40°$) was chosen closest to the symmetric pair of angles which allowed $p_5=0$, the average recoil momenta of the measured energy sharing spectra are slightly larger than zero (4.4 MeV/c at 250 MeV, 6.7 MeV/c at 350 MeV, and 9.7 MeV/c at 500 MeV). The data at 250, 350, and 500 MeV represent a maximum angular acceptance $\Delta\theta=\pm 1.5°$ and $\Delta\phi=\pm 1.0°$, $\Delta\theta=\pm 1.7°$ and $\Delta\phi=\pm 1.3°$, and $\Delta\theta=\pm 1.5°$ and $\Delta\phi=\pm 1.1°$, respectively. The quantity $\Delta\theta$ is the vertical opening angle as seen from the target center. The error bars are for counting statistics only. The energy

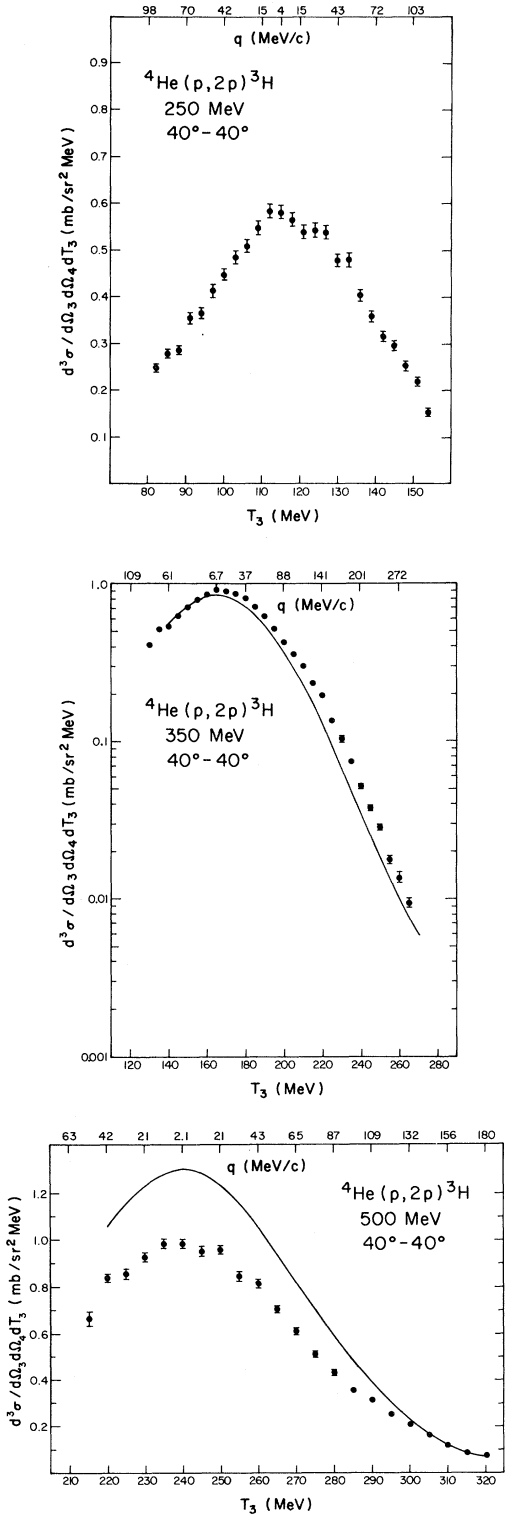

FIG. 3. Energy sharing spectra for the ^{4}He$(p,2p)^3$H reaction at 250, 350, and 500 MeV. The abscissae give both the energy of one of the observed protons and the recoil momentum of the core nucleus.

sharing spectra have the typical shape expected for knockout of an *s*-state proton. The differential cross sections at the above values of p_5 (with the restriction that $\Delta\theta = \pm 0.5°$ and $\Delta\phi = \pm 0.5°$) are compared with previous results at lower and higher energies in Fig. 4. A smooth behavior as a function of energy is apparent. There is good agreement with the 590 MeV result of Perdrisat *et al.* [4]

The coplanar symmetric angular distributions measured at 350 and 500 MeV are shown in Fig. 5. The angular pairs $\theta_3 = \theta_4$ ranged from 30° to 64°. The data reflect an angular acceptance of $\Delta\theta = \pm 0.5°$ and $\Delta\phi \simeq \pm 1.3°$ at each angle, except that at 350 MeV the angular spread in $\Delta\theta$ at 64° is $\pm 1.1°$ and at 500 MeV the angular spread in $\Delta\theta$ for angles greater than 57° ranges from $\pm 0.7°$ to $\pm 1.7°$. Note that the 350 MeV data extend to recoil momenta of 410 MeV/*c* and that the 500 MeV data extend to recoil momenta of 490 MeV/*c*. This is a considerably larger range than has ever been obtained previously for the $(p,2p)$ reaction on any nucleus. Note further that the differential cross sections span a difference of almost five orders of magnitude. The distorted momentum distribution determined from the 500 MeV coplanar symmetric angular distribution by dividing by $F(d\sigma/d\Omega)_1^p {}_2^p N_p$ is compared with that obtained from the 590 MeV data by Perdrisat *et al.*[4] in Fig.

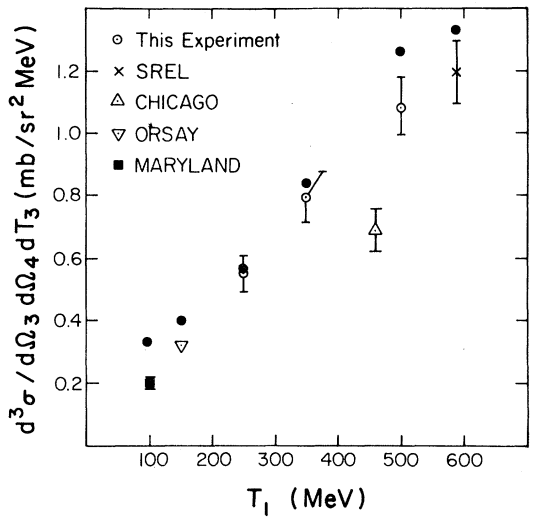

FIG. 4. Energy dependence of the differential cross section for the ^{4}He$(p,2p)^3$H reaction at zero-recoil momentum and symmetric angles. The symbols indicate the results of: the present experiment (●); obtained at SREL (×), Ref. 4; at Chicago (△), Ref. 3; at Orsay (▽), Ref. 2; and at Maryland (■), Ref. 1. The full circles present the results of a DWIA calculation.

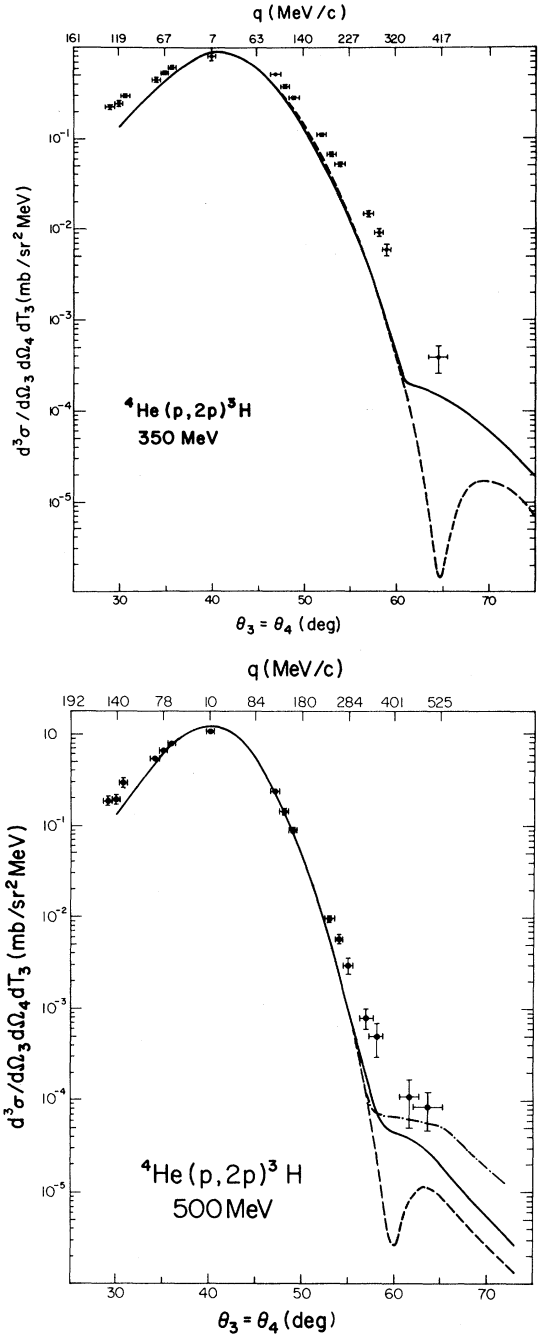

FIG. 5. Coplanar symmetric angular distributions for the ^{4}He$(p,2p)^3$H reaction at 350 and 500 MeV. The abscissae give both the scattering angles $\theta_3=\theta_4$ of the observed protons and the recoil momentum of the core nucleus. The curves correspond to DWIA predictions for the meson exchange currents corrected wave function with spin-orbit terms (solid line) and without spin-orbit terms (dashed line) in the optical potentials. The dot-dash curve (500 MeV) corresponds to the DWIA prediction for the Lim wave function with spin-orbit terms in the optical potentials.

6. The half-off-the-energy-shell proton-proton differential cross section $(d\sigma/d\Omega)_{1/2}^{p}$ was replaced by the free p-p differential cross section at a c.m. energy corresponding to the c.m. energy of the two protons in the final state. The c.m. scattering angle is the angle between the relative momentum vector of the two protons in the final state and the incident beam direction ($=90°$ for a coplanar symmetric angular distribution. This approximation for $(d\sigma/d\Omega)_{1/2}^{p}$ is the so-called final state approximation. There appears to be good agreement in magnitude and shape between the two distorted momentum distributions, except perhaps for angles $\theta_3=\theta_4\leq 30°$ or $q\geq 100$ MeV/c antiparallel to the beam direction.

Four point quasifree angular distributions were obtained at 250 and 500 MeV. The angle pairs at which measurements were made are $25°-55°$, $30°-50°$, $35°-45°$, and $40°-40°$. In addition to an unpolarized beam, a polarized proton beam was used; however, only the differential cross sections are considered here. The energy spectra for these asymmetric angle pairs are shown in Fig. 7. The energy spectra are presented as functions of

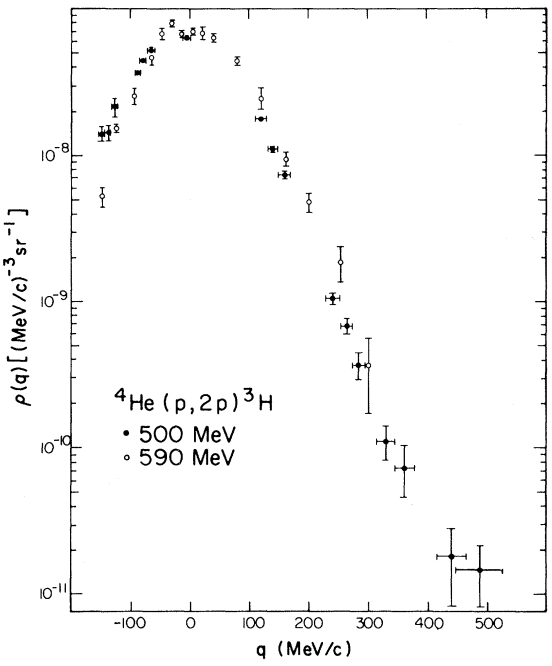

FIG. 6. Distorted momentum distributions obtained from the 500 MeV (present work) and 590 MeV (Ref. 4) coplanar symmetric angular distributions using the final state energy prescription to approximate the half-off-the-energy-shell p-p differential cross sections and assuming factorization of cross sections.

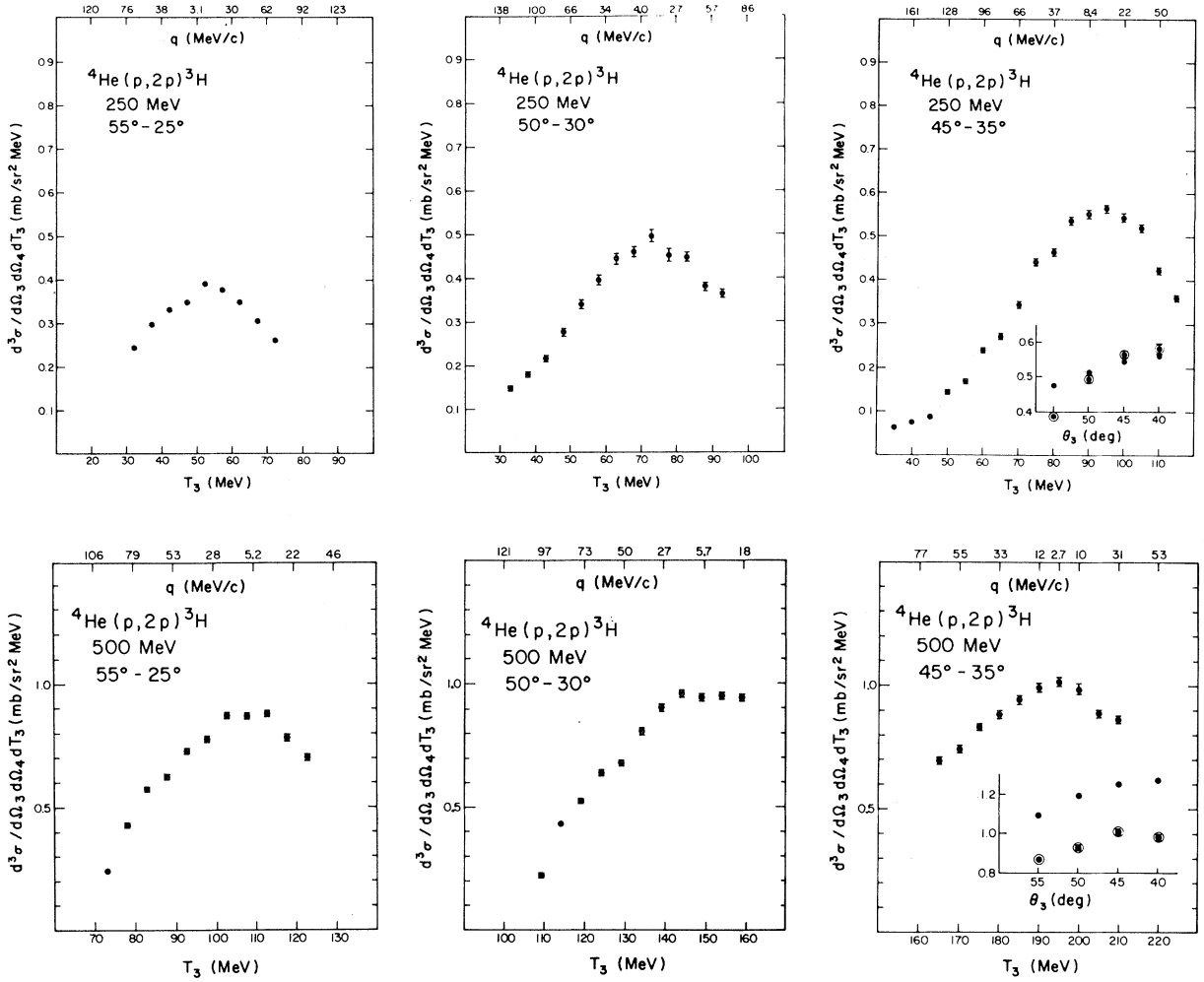

FIG. 7. Energy spectra for the ^{4}He$(p,2p)^3$H reaction at the angle pairs 55°−25°, 50°−30°, and at 45°−35° at 250 and 500 MeV. The inserts show four point quasifree angular distributions (dots with error bars) compared with DWIA calculations (solid dots).

energy of the proton detected at the larger angle and as a function of the recoil momentum of the core nucleus. The energy spectra have the expected shape for knockout of an *s*-state proton. Data in numerical form may be obtained by request from the authors.

V. DWIA CALCULATIONS

DWIA calculations were made similar to those of Roos.[9] The computer code used was written by Chant[10] and is based upon the formulations of Jackson and Berggren, and Jackson.[11] Its main difference with earlier DWIA codes is that it allows the distorted waves to be generated from an optical potential which contains a complex spin-orbit term as well as an *l*-dependent term. For purposes of comparison, we first discuss the main ingredients of DWIA calculations for a quasifree $(p,2p)$ reaction assuming factorization of cross sections, i.e., neglecting spin-orbit terms of the optical potentials. The main ingredients in this case are (i) the half-off-the-energy-shell p-p differential cross section, and (ii) the distorted momentum distribution. The latter is calculated from a single particle wave function representing the overlap of ^{4}He and ^{3}H wave functions with distorted waves for the incident proton, the scattered proton, and ejected proton.

A. The half-off-the-energy-shell p-p differential cross section

This quantity is usually replaced by the free p-p cross section using one of the following approximations:

(a) *The initial state approximation.* In this approximation, the free p-p differential cross section is taken at a c.m. energy equal to the c.m. energy of the incident proton and the struck proton (laboratory momenta $\vec{p}_1$ and $-\vec{p}_5$):

$$E_1'+\bar{E}_4'=(1-\beta_{14}^2)^{1/2}(E_1+\bar{E}_4)\ ,$$

with

$$\vec{\beta}_{14}=\frac{\vec{p}_1-\vec{p}_5}{E_1+\bar{E}_4}$$

and

$$\bar{E}_4=[(-\vec{p}_5)^2+m_4^2]^{1/2}\ .$$

The c.m. scattering angle is defined through

$$\cos\theta_3'=\frac{\vec{p}_1'\cdot\vec{p}_3'}{|\vec{p}_1'|\ |\vec{p}_3'|}\ ,$$

where $\vec{p}_1'$ and $\vec{p}_3'$ are obtained through the Lorentz transformation defined above.

(b) *The final state approximation.* In this approximation, the free p-p differential cross section is taken at a c.m. energy equal to the c.m. energy of the scattered proton and the ejected proton.

$$E_3'+E_4'=(1-\beta_{3,4}^2)^{1/2}(E_3+E_4)\ ,$$

with

$$\vec{\beta}_{3,4}=\frac{\vec{p}_3+\vec{p}_4}{E_3+E_4}\ .$$

The c.m. scattering angle is defined as above.

(c) *The Stern-Chamberlain approximation (Ref. 12).* In this approximation, one conserves the difference Q and the sum P of the initial and final relative momenta of the two interacting protons:

$$\vec{Q}=\tfrac{1}{2}(\vec{K}-\vec{K}'),\quad \vec{P}=\tfrac{1}{2}(\vec{K}+\vec{K}')\ ,$$

where

$$\vec{K}=\vec{p}_1+\vec{p}_5\ ,\quad \vec{K}'=\vec{p}_3-\vec{p}_4\ .$$

Nonrelativistically, this corresponds to p-p scattering at a c.m. energy with a relative momentum $p_{\rm rel}$ and scattering angle θ given by

$$|\vec{Q}|^2=2p_{\rm rel}^2(1-\cos\theta)\ ,$$

$$|\vec{P}|^2=2p_{\rm rel}^2(1+\cos\theta)\ .$$

At the energies of the present experiment, the differences caused by the particular choice of the free p-p differential cross section are small for recoil momenta up to 200 MeV/c. For instance, the differences in the distorted momentum distributions for recoil momenta up to 200 MeV/c obtained assuming the factorization of cross sections are less than 15%. For increasing recoil momenta the differences in the distorted momentum distributions become increasingly larger, as can be seen in Fig. 8. The expected result for the Stern-Chamberlain approximation is intermediate to the initial state energy approximation and the final state energy approximation results.

The other possibility is to calculate the half-off-the-energy-shell t matrix using some potential model. Here, one writes the half-off-the-energy-shell extension function multiplied by the on-the-energy-shell t matrix.

$$t(q,q_{\rm el},E)=f(q,q_{\rm el})t(q_{\rm el},q_{\rm el},E)\ .$$

The second term $t(q_{\rm el},q_{\rm el},E)$ can be calculated knowing the p-p elastic scattering phase shifts, while the first term $f(q,q_{\rm el})$, the off-the-energy-shell extension function, may be calculated from some potential model.[13] No such potential is avail-

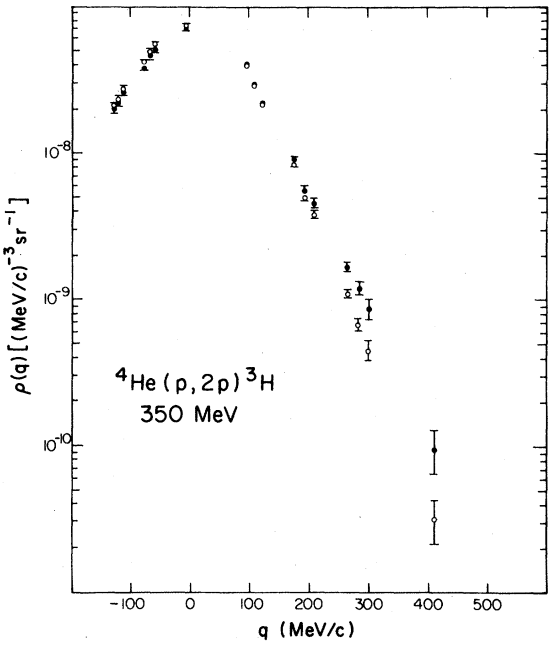

FIG. 8. Distorted momentum distributions obtained from the 350 MeV coplanar symmetric angular distribution using the initial state and final state energy prescriptions and assuming factorization of cross sections.

able for the range of p-p c.m. energies relevant to the present experiment.

When the spin dependent parts of the optical potentials are included, one retains factorization of amplitudes rather than factorization of cross sections. The differential cross section can then be expressed as

$$d^3\sigma/(d\Omega_3 d\Omega_4 dT_3) = FS_{\rm fi} \mid T_{\rm fi} \mid^2 ,$$

where F is the kinematic factor and $S_{\rm fi}$ represents the appropriate sum and average over final- and initial-state quantum numbers, and

$$T_{\rm fi} = \sum_{\sigma_2} C \sum_{\mu_1\mu_3\mu_4} \langle \mu_3\mu_4 \mid t_{pp} \mid \mu_1\sigma_2 \rangle \times \int \chi^{(-)*}_{\mu_3\sigma_3}(\vec{r}) \chi^{(-)*}_{\mu_4\sigma_4}(\vec{r}) \phi(\vec{r}) \times \chi^{(+)}_{\mu_1\sigma_1}(\alpha\vec{r}) d\vec{r} .$$

Here, $\langle \mu_3,\mu_4 \mid t_{pp} \mid \mu_1,\sigma_2 \rangle$ presents the p-p scattering amplitude. The (μ_i,σ_i) present the spin quantum numbers of particle i. The impulse approximation kinematics are defined as above.

Unless otherwise stated, the DWIA calculations presented here have been made using the final-state approximation. The free p-p scattering amplitudes have been obtained from a set of phase shifts for p-p elastic scattering up to 700 MeV (Ref. 14) and at higher energies by interpolation of p-p differential cross section data given in a recent compilation.[15]

B. Distorted waves

In order to arrive at a consistent set of optical model parameters appropriate to generate distorted waves for the incident and outgoing channels, an optical model analysis was made of available $p+{}^4$He, $p+{}^3$He, and $p+{}^3$H elastic scattering data in the energy range 85 MeV$-$1.24 GeV. For the incident channel, the proper optical potential is for the incident particle and core nucleus. In the present DWIA calculations, this interaction was replaced by a $p+{}^4$He optical potential. The data selection is presented in Table I. Only two total reaction cross sections were found in the literature for the energy range under consideration: at 630 ± 15 MeV, $\sigma_R(p+{}^4\text{He}) = 12.6\pm1.4$ fm^2 (Ref. 16) and at 1030 MeV, $\sigma_R(p+{}^4\text{He}) = 11.1\pm1.0$ fm^2 (Ref. 17). The analysis was performed using the optical model search code SEEK.[18] The optical potential is of the form

$$V = V_{\rm Coul} - Vf(r,R_R,a_R) - iWf(r,R_I,a_I) - (V_{\rm SO}+iW_{\rm SO})g(r,R_{\rm SO},a_{\rm SO},)(\vec{s}\cdot\vec{l}) - (-1)^l(V_{\rm ex}+iW_{\rm ex})f(r,R_{\rm ex},a_{\rm ex}) ,$$

containing a Coulomb potential term, a real central and imaginary central potential term, a complex spin-orbit potential term with a Thomas form, and a complex l-dependent potential term. The form factors $f(r,R,a)$ and $g(r,R,a)$ are the usual Wood-Saxon and Thomas form factors:

$$f(r,R_i,a_i) = \left| 1+\exp\left[\frac{r-R_i}{a_i}\right]\right|^{-1} ,$$

$$g(r,R_i,a_i) = -\frac{2}{r}\left[\frac{\hbar}{m_\pi c}\right]^2 \frac{df(r,R_i,a_i)}{dr} ,$$

with

$$R_i = r_i A^{1/3} .$$

The quantities $\vec{s}$ and $\vec{l}$ denote the spin and orbital angular momentum of the incident nucleon. The Coulomb potential term is taken to be due to a uniformly charged sphere with radius parameter r_C determined by electron scattering data. Corrections for relativistic effects were introduced as previously[19] by performing the calculations with the correct wave number k and by dividing the strengths of the central potential terms obtained using the nonrelativistic Schrödinger equation by a correction factor γ.

The optical potential contains a total of 14 adjustable parameters to be determined by fitting the data. Guess values used as starts in the searches were taken from previous analyses of the data referenced in Table I and from an analysis by Leung and Sherif.[20] The procedure followed, in general, was to first search on the potential strengths V, W, $V_{\rm SO}$, and $W_{\rm SO}$ and then with the new values of V, W, $V_{\rm SO}$, and $W_{\rm SO}$ held fixed to search on the dynamical parameters r_R, a_R, r_I, and a_I. This process was repeated at least once but often several times, each time starting with the new parameters. At those energies where analyzing power data are available, the spin-orbit geometry parameters $r_{\rm SO}$ and $a_{\rm SO}$ were included in the searches starting with the second cycle. After these searches had sufficiently converged, all-parameter searches were made with the l-dependent potential set equal to zero. Finally, at those energies where the differential cross section angular distribution spans the whole range from extreme for-

TABLE I. Data selection for the optical model analysis of $p+^4$He, $p+^3$He, and $p+^3$H.

T	$\sigma(\theta)$	$A(\theta)$	Ref.	T	$\sigma(\theta)$	$A(\theta)$	Ref.
$p+^4$He							
85	×		a	600	×		j
100	×		b	650	×		f
147	×[o]	×[o]	c	720	×		i
156	×		d	788	×		g
200	×	×	e	800	×	×	h
350	×		f	1029	×	×	h
350	×	×	e	1050	×[p]		f
400	×		g	1150	×[p]		f
500	×	×	e	1240	×	×	h
561	×	×	h				
580	×		i				
$p+^3$He							
85	×		a	600	×		j
100	×		b	715	×		l
156.5	×		k	1000	×		m
415	×		l				
$p+^3$H							
156.5	×		k				
415	×		n				
600	×		j				

[a]L. G. Volta *et al.*, Phys. Rev. C 10, 520 (1974).
[b]N. P. Goldstein *et al.*, Can J. Phys. 48, 2629 (1970).
[c]A. M. Cormack *et al.*, Phys. Rev. 115, 599 (1959).
[d]V. Comparat *et al.*, Phys. Rev. C 12, 251 (1975).
[e]L. G. Greeniaus *et al.*, Phys. Rev. C 21, 1932 (1980).
[f]G. Bruge, J. Phys. (Paris) 40, 635 (1979).
[g]G. J. Igo, private communication.
[h]H. Courant *et al.*, Phys. Rev. C 19, 105 (1979).
[i]S. L. Verbeck *et al.*, Phys. Lett. 59B, 339 (1975).
[j]J. Fain *et al.*, Nucl. Phys. A262, 413 (1976).
[k]H. Langevin-Joliot *et al.*, Nucl. Phys. A158, 309 (1970).
[l]R. Frascaria *et al.*, Contribution to the Seventh International Conference on High Energy Physics and Nuclear Structure, Zürich, 1977 (unpublished).
[m]R. Frascaria *et al.*, Nucl. Phys. A264, 445 (1976).
[n]G. Bizard *et al.*, Nucl. Phys. A338, 451 (1980).
[o]The differential cross sections and polarizations have been multiplied by renormalization factors of 1.11 and 0.933, respectively. [See J. N. Palmieri *et al.*, Phys. Lett. 6, 289 (1963) and O. N. Jarvis and B. Rose, *ibid.* 15, 271 (1965).]
[p]The 1050 and 1150 MeV differential cross sections have been multiplied by factors 0.650 and 0.685, respectively, to obtain a consistent normalization in the energy range 500 MeV − 1.24 GeV.

TABLE II. Optical-model parameters from least-squares searches of $p+{}^4$He elastic scattering data in the energy range 85–1240 MeV, and of $p+{}^3$He and $p+{}^3$H elastic scattering in the energy range 85–1000 MeV. The quantities N_σ and N_A refer to the number of experimental differential cross sections and analyzing powers, respectively, while the quantity N^{-1} is the normalization factor to the differential cross sections, suggested by the least-squares search. All other quantities are defined in the text. The parameters in parentheses were kept fixed during the search.

T (MeV)	V (MeV)	r_R (fm)	a_R (fm)	W (MeV)	R_I (fm)	a_I (fm)	V_{SO} (MeV)	W_{SO} (MeV)	r_{SO} (fm)
$p+{}^4$He, $r_C=1.36$ fm									
85	15.47	1.092	0.429	17.01	1.563	0.343	11.37	1.88	1.048
100	−2.80	1.396	0.404	10.31	1.696	0.260	10.31	−0.40	1.034
147	5.47	1.489	0.983	11.39	1.513	0.293	6.02	−3.81	0.843
156	−3.56	2.391	0.001	9.34	1.831	0.139	6.18	−2.31	1.018
200	1.08	2.485	0.102	15.01	1.492	0.299	6.45	−4.01	0.834
350	−15.06	1.395	0.206	18.01	1.692	0.258	5.18	−0.33	(1.049)
350	−3.33	1.525	0.003	8.42	1.972	0.130	6.02	−5.30	0.872
400	−11.38	1.525	0.157	45.58	1.629	0.433	4.99	0.00	(1.049)
500	−1.43	1.867	0.008	45.22	1.208	0.443	4.69	−7.97	0.845
561	−23.03	1.117	0.275	58.50	0.946	0.461	5.75	−5.12	0.885
580	−11.50	1.470	0.269	18.76	1.833	0.351	4.76	0.56	(1.049)
600	−10.33	1.534	0.157	34.10	1.919	0.397	7.51	0.09	(1.049)
650	−12.19	1.503	0.193	22.68	1.826	0.367	5.28	−0.10	1.049
720	−10.25	1.505	0.100	18.30	1.780	0.459	4.53	0.01	(1.049)
788	−1.37	1.020	0.019	97.79	1.008	0.280	3.40	−3.98	0.780
800	4.55	1.819	0.506	88.54	1.078	0.284	1.42	−5.50	0.849
1029	−4.79	1.106	0.020	81.54	1.110	0.256	1.22	−4.40	0.837
1050	−54.35	0.930	0.245	109.12	1.034	0.307	2.73	−3.69	0.819
1150	−36.06	0.954	0.101	91.39	1.074	0.288	3.26	−3.78	0.824
1240	−10.17	1.150	0.002	88.07	1.113	0.274	2.76	−6.07	0.630
$p+{}^3$He, $r_C=1.30$ fm									
85	7.17	1.679	0.228	10.34	1.993	0.011	7.19	−6.40	1.086
100	−8.86	1.390	0.592	8.50	1.916	0.000	10.68	−0.96	1.040
156.5	10.46	1.341	0.011	15.22	1.439	0.320	0.39	4.79	0.852
415	12.32	1.544	0.155	10.64	1.832	0.174	3.18	−0.85	(1.049)
600	−8.57	1.413	0.090	(11.00)	1.673	0.167	3.05	−1.43	(1.049)
715	−9.04	1.392	0.014	13.50	1.368	0.470	3.09	−0.33	(1.049)
1000	−25.80	1.302	0.183	(15.00)	2.074	0.359	1.57	−1.08	(1.049)
$p+{}^3$H, $r_C=1.30$ fm									
156.5	6.97	1.474	0.100	10.40	1.728	0.248	4.48	−0.18	1.050
415	20.72	1.405	0.287	9.85	1.811	0.245	2.31	−0.42	(1.049)
600	−56.42	1.069	0.318	(13.00)	1.769	0.339	−0.10	(−0.61)	(1.049)

ward to extreme backward angles, the l-dependent potential parameters were searched on together with all the other parameters starting at the previous best fit values. The strength of the imaginary part of the l-dependent potential term was set equal to zero.

The best fit parameters are presented in Table II. Fits which yielded parameters giving unreasonable values for the total reaction cross section were discarded. The 400 and 600 MeV optical model parameters given in Table II are the most reasonable sets, although the predicted values for the total reaction cross sections are rather large. It is to be noticed that, in general, the results are not very satisfactory, possibly reflecting the uncertainties in the normalization and the zero of the angular

TABLE II. (*Continued.*)

a_{SO} (fm)	V_{ex} (MeV)	r_{ex} (fm)	a_{ex} (fm)	N^{-1}	χ_σ^2	N_σ	χ_A^2	N_A	σ_R^{th} (fm^2)
0.236	−3.917	(0.930)	0.768	0.999	365	42			18.86
0.299	0.051	1.117	0.400	0.979	1384	33			13.84
0.206	−0.008	(0.930)	(0.299)	1.001	2299	33	1632	33	9.32
0.278	−0.704	(0.930)	0.552	0.985	376	41			11.62
0.240	0.301	(0.930)	0.269	0.989	2102	47	1392	40	9.92
(0.289)	(0.000)			1.004	6832	85			12.77
0.405	0.070	(0.930)	1.281	1.012	10175	38	19988	38	8.55
(0.289)	(0.000)			1.003	526	22			24.25
0.344	0.226	(0.930)	0.197	1.018	10008	44	6343	44	11.00
0.341	(0.000)			1.010	103	44	249	44	8.69
(0.289)	(0.000)			0.997	269	43			14.45
(0.289)	(0.000)			0.998	129	46			24.76
0.289	(0.000)			0.998	170	33			15.94
(0.289)	(0.000)			0.991	366	41			13.40
0.277	0.122	0.122	1.134	0.999	789	200			8.81
0.264	(0.000)			1.033	331	32	1017	32	9.21
0.303	(0.000)			1.064	375	34	972	33	8.30
0.282	(0.000)			1.003	119	89			9.54
0.309	(0.000)			1.000	48	40			8.59
0.457	(0.000)			1.108	1618	20	319	20	8.52
0.222	−2.673	(0.930)	0.749	1.018	120	28			13.88
0.296	−2.344	(0.930)	0.494	1.015	72	22			11.18
0.232	−1.167	(0.930)	0.572	0.995	586	25			8.54
(0.289)	(0.000)			0.963	2094	70			7.41
(0.289)	(0.000)			1.023	1761	60			4.84
(0.289)	(0.000)			1.036	341	57			4.78
(0.289)	(0.000)			0.992	90	25			10.50
0.270	−2.079	(0.930)	0.433	1.008	383	25			9.87
(0.289)	(0.000)			1.151	438	11			7.15
(0.289)	(0.000)			1.003	247	40			7.65

scales of the data. Most prominent are the scatter in the values of the strengths of the real central (V) and imaginary spin-orbit (W_{SO}) potential terms. In many cases the fits to the experimental data are marginal. It should be remarked that the optical model as used in the present analysis is not expected to provide a very realistic description of proton-light nucleus elastic scattering. It was shown in a recent optical model analysis of 200 MeV, $p+^{12}$C and $p+^{13}$C elastic scattering data that much better fits are obtained when the attractive Woods-Saxon real central potential term is replaced by a combination of two Woods-Saxon potential terms giving repulsion at the center and attraction at larger radii.[21]

To obtain an energy dependent average parameter set, the following quantities were determined:

$$\gamma J_R'/A = \left[\int V_R(r) d^3r \right] / A$$

$$\simeq \frac{4\pi}{3} V r_R^3 \left[1 + \frac{\pi^2 a_R^2}{r_R^2 A^{2/3}} \right],$$

$$\langle r^2\rangle_R{}^{1/2}=\left|\frac{\int r^2V(r)d^3r}{\int V(r)d^3r}\right|^{1/2}$$
$$\simeq\frac{1}{\sqrt{5}}(3r_R{}^2A^{2/3}+7\pi^2a_R{}^2)^{1/2}\ ,$$

where $\gamma J_R'/A$ and $\langle r^2\rangle_R{}^{1/2}$ are the volume integral per nucleon and the rms radius, respectively, of the real central potential. Similarly, for the imaginary central potential, the quantities $\gamma J_I'/A$ and $\langle r^2\rangle_I{}^{1/2}$ were calculated. The correction factor γ follows from the multiplicative factor to the strengths of the real and imaginary central potential terms for a Dirac particle in a central field. (The entries in Table II for V and W are those obtained with the nonrelativistic optical model code; they should read $V=\gamma V'$ and $W=\gamma W'$, respective-

TABLE III. rms radii for the real central and imaginary central potential terms and volume integrals per nucleon of the real central, imaginary central, real spin-orbit, and imaginary spin-orbit potential terms. γ is the relativistic correction term to the central potential terms.

T (MeV)	γ	$\gamma J_R'/A$ (MeV fm^3)	$\langle r^2\rangle_R{}^{1/2}$ (fm)	$\gamma J_I'/A$ (MeV fm^3)	$\langle r^2\rangle_I{}^{1/2}$ (fm)	J_{SO_R}/A (MeV fm^3)	J_{SO_I}/A (MeV fm^3)
$p+{}^4$He							
85	1.059	135.4	2.085	323.4	2.306	237.7	55.2
100	1.069	−42.4	2.281	230.0	2.298	212.7	−8.3
147	1.100	204.8	4.087	189.5	2.156	101.2	−64.1
156	1.106	−203.8	2.940	245.6	2.310	125.5	−46.9
200	1.134	69.6	3.079	241.6	2.145	107.3	−66.7
350	1.228	−185.9	1.878	398.6	2.291	108.4	−6.9
350	1.228	−49.5	1.875	275.0	2.472	104.7	−92.2
400	1.258	−176.0	1.964	1053.5	2.570	104.4	0
500	1.317	−39.0	2.296	509.7	2.218	79.1	−134.4
561	1.352	−166.3	1.712	400.3	2.221	101.5	−90.4
580	1.362	−173.0	2.066	553.3	2.604	99.6	11.7
600	1.373	−162.6	1.974	1178.0	2.783	157.1	1.9
650	1.401	−184.5	1.982	669.8	2.627	110.5	−2.1
720	1.438	−148.9	1.888	554.8	2.775	94.8	0.2
788	1.474	−6.7	1.256	545.9	1.618	52.8	−61.9
800	1.481	149.5	2.922	590.8	1.695	24.0	−93.0
1029	1.595	−27.2	1.362	564.3	1.664	20.4	−73.6
1050	1.605	−232.8	1.462	679.6	1.708	44.6	−60.3
1150	1.653	−136.9	1.232	607.7	1.700	53.6	−62.1
1240	1.694	−64.8	1.414	629.2	1.706	34.7	−76.3
$p+$3He							
85	1.053	154.6	2.058	342.9	2.227	188.7	−168.1
100	1.062	−185.5	2.693	250.4	2.140	268.4	−24.1
156.5	1.095	105.7	1.499	234.5	2.000	8.0	98.6
415	1.239	199.0	1.819	285.8	2.146	80.6	−21.5
600	1.333	−103.6	1.620	226.0	1.969	77.3	−36.2
715	1.388	−102.2	1.556	225.8	2.321	78.3	−8.0
1000	1.515	−260.8	1.605	640.1	2.674	39.8	−27.4
$p+{}^3$H							
156.5	1.095	95.5	1.688	246.7	2.139	113.7	−4.4
415	1.239	288.4	1.898	266.3	2.219	58.6	−10.7
600	1.323	−409.9	1.680	354.0	2.344	−2.5	−15.5

ly.) The results obtained for the volume integral per nucleon and the rms radius of the real and imaginary central potential terms are presented in Table III. Also entered are the volume integrals per nucleon of the real and imaginary parts of the spin-orbit potential term:

$$\frac{J_{SO_R}}{A}+\frac{iJ_{SO_I}}{A}=\frac{\int[V_{SO}(r)+iW_{SO}(r)]d^3r}{A}$$

$$\simeq 8\pi\left[\frac{\hbar}{m_\pi c}\right]^2(V_{SO}+iW_{SO})r_{SO}A^{-2/3}.$$

One then obtains from Table II the average diffuseness parameters $\bar{a}_R$, $\bar{a}_I$, $\bar{a}_{SO}$, and $\bar{a}_{ex}$. The rms radii and the energy dependence of the volume integrals follow from Table III. The latter, together with the diffuseness parameters, determine the radius parameters r_R, r_I, and r_{SO}, and the energy dependence of the potential strengths V, W, V_{SO}, and W_{SO}.

(a) $p+^4$He, $85<T<1240$ MeV. $\bar{a}_R=0.200$ fm; $\langle r^2\rangle_R^{1/2}=2.077$ fm or $r_R=1.577$ fm; $V=[27.35-5.046\ln(T)]$ MeV. $\bar{a}_I=0.315$ fm; $\langle r^2\rangle_I^{1/2}=2.177$ fm or $r_I=1.493$ fm; $W=(6.55+6.977\times10^{-2}T-6.250\times10^{-5}T^2+2.3215\times10^{-8}T^3)$ MeV. $\bar{a}_{SO}=0.303$ fm; $\bar{r}_{SO}=0.879$ fm; $V_{SO}=[25.37-3.243\ln(T)]$ MeV; $W_{SO}=[5.69-1.355\ln(T)]$ MeV; $\bar{a}_{ex}=0.657$ fm; $r_{ex}=0.930$ fm; V_{ex} can be obtained by graphical interpolation.

(b) $p+^3$H, $85<T<1000$ MeV.

The paucity of $p+^3$H data compelled the analysis of $p+^3$H together with $p+^3$He elastic scattering data. This approach may be justified as far as the geometry is concerned, since the charge and magnetic radii of ^{3}H and ^{3}He do not differ greatly [for ^{3}H, $\langle r^2\rangle_{ch}^{1/2}=1.70\pm0.05$ fm, $\langle r^2\rangle_{mag}^{1/2}=1.70\pm0.05$ fm, and for ^{3}He, $\langle r^2\rangle_{ch}^{1/2}=1.844\pm0.045$ fm, $\langle r^2\rangle_{mag}^{1/2}=1.74\pm0.10$ fm (Ref. 22)]. However, the strengths of the various potential terms will be different due to the difference in the p-p and p-n interactions. This difference may be accounted for through a $(\vec{t}_1\cdot\vec{t}_2)$ term in the optical potential. The quantities $\vec{t}_1$ and $\vec{t}_2$ are the isospins of the incident proton and the target nucleus, respectively. Unfortunately, the scatter in the strengths of the potential terms do not allow such a distinction to be made at present. $\bar{a}_R=0.199$ fm; $\overline{\langle r^2\rangle^{1/2}}=1.812$ fm; $r_R=1.481$ fm; $V=[67.01-11.91\ln(T)]$ MeV. $\bar{a}_I=0.233$ fm; $\overline{\langle r^2\rangle_I^{1/2}}=2.218$ fm; $r_I=1.828$ fm; $W=[12.65-2.478\times10^{-2}T+3.413\times10^{-5}T^2]$ MeV. $\bar{a}_{SO}=0.255$ fm; $\bar{r}_{SO}=1.007$ fm; $V_{SO}=[17.47-2.343\ln(T)]$ MeV; $\overline{W_{SO}}=-0.76$ MeV; $\bar{a}_{ex}=0.562$ fm; $r_{ex}=0.930$ fm; again V_{ex} can be obtained by graphical interpolation.

Since $p+^3$H optical model parameters are needed corresponding to incident energies less than 85 MeV, a further analysis was made of $p+^3$He differential cross section and analyzing power data at 30.0, 40.0, and 47.6 MeV.[23] With the latter optical model parameter sets, it was possible to make an interpolation for the energy region 30–85 MeV.

One should note the rather small diffuseness parameters of both energy-dependent average parameter sets. Small diffuseness parameters were also found in the analysis of Leung and Sherif[20] as well as in analyses of low-energy p-^{3}He and p-^{4}He elastic scattering data[24] and are consistent with what is found for other light nuclear systems. The rms radii of the real central potential are somewhat larger than the rms charge radii as to be expected; for ^{4}He, $\langle r^2\rangle_{ch}^{1/2}=1.674\pm0.012$ fm.[25] The DWIA calculations presented here have been made using the energy-dependent average optical model parameter sets, except that for $p+^3$H the strength of the imaginary central potential (W) was fixed at 11.0 MeV for energies above 100 MeV.

A few additional comments need to be made regarding the energy-dependent average parameter set for $p+^4$He elastic scattering. First, there is some noticeable energy dependence in rms radius of the real central potential with larger values at the lower energies and smaller values at the higher energies. This was also remarked by Leung and Sherif[20] and points to the deficiencies of the optical model. Second, the strength of the real central potential changes sign around 225 MeV, which is somewhat lower than obtained in optical model analyses of proton elastic scattering of medium weight and heavy nuclei.[19] Third, there is a gradual increase in the strength of the imaginary central potential term, as one would expect because of pion production. Fourth, the spin orbit potential term is complex with the strength of the real part decreasing with energy and the strength of the imaginary part slowly increasing with energy, while the signs are opposite. There is no change in the sign of either part in the energy range under consideration. Finally, the strength of the l-dependent potential term is negative up to about 175 MeV after which it attains a small positive value. The behavior of the strength of the real part of the l-

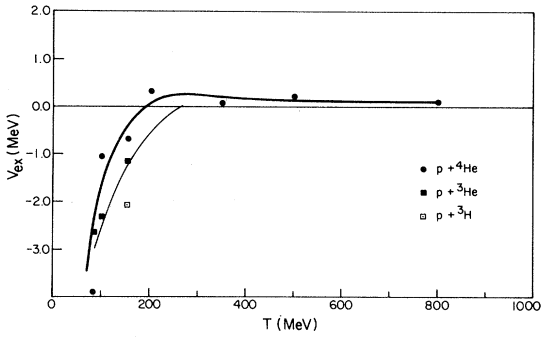

FIG. 9. Strengths of the real l-dependent term of the optical potential. The solid lines are to indicate the trend of the results.

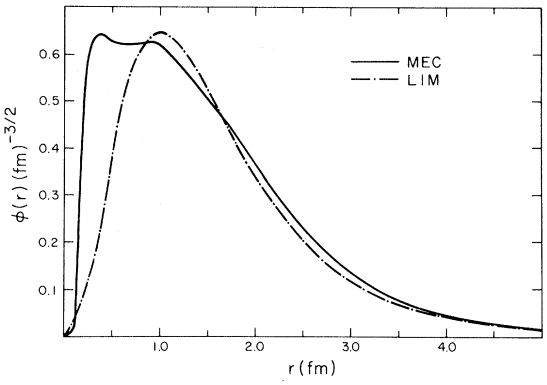

FIG. 10. Single-particle wave functions used in the DWIA calculations. MEC is the wave function obtained in fitting the ^{3}He charge form factor with corrections for meson exchange current effects. The second wave function is of Eckart form (Refs. 24 and 32).

dependent potential term with energy for $p+{}^4$He and $p+{}^3$He is shown in Fig. 9.

C. Single-particle wave function

This function can be obtained theoretically by computing three- and four-body wave functions for ^{3}H and ^{4}He and using these in the overlap integral. However, because of the complexity of such calculations, and the necessity of severe approximations in these, it has become customary to derive the overlap function from data on electron-^{4}He scattering using a simple model for the ^{4}He nucleus. One then assumes[26] that the ^{4}He wave function can be represented by a product of the ^{3}H internal wave function and the p-^{3}H relative wave function $\phi(\vec{r})$, so that the one-body density and therefore the ^{4}He charge form factor is a simple integral over $|\phi(\vec{r})|^2$:

$$F_{\rm ch}(q^2)=F_N(q^2)\int \exp(i\tfrac{3}{4}\vec{q}\cdot\vec{r})\,|\phi(\vec{r})|^2 d\vec{r}\,,$$

where $F_N(q^2)$ is the isoscalar nucleon form factor. Using a simple Eckart parametrization of the wave function

$$\phi(\vec{r})=N\frac{1}{r}\exp(-\alpha r)[1-\exp(-\beta r)]^n\,,$$

Lim[26] obtained $n=4$ and $\beta=1.2$ fm^{-1}, whereas Lesniak *et al.*[27] obtained $n=4$ and $\beta=1.42$ fm^{-1}. In the latter case, it is not clear how the nucleon form factor is treated. Recently, this approach has come under attack[28] because of the neglect of meson exchange corrections in e-^{4}He scattering. In order to correct for these effects, Shepard *et al.*[29] fitted existing theoretical predictions[30] for the one-body part of the charge form factor. An alternative approach is to obtain new "experimental" data on the charge form factor by subtracting the meson exchange contribution as given by theory. Since this approach seems least vulnerable to theoretical uncertainties, this approach was followed, employing the meson exchange calculations of Gari *et al.*[30] A second difference with the calculation of Shepard *et al.*[29] is that a more flexible form for the p-t wave function was used:

$$\phi(\vec{r})=\frac{1}{r}\sum_{i=1}^{5}\alpha_i\exp(-\beta_i r)\,,$$

with the correct asymptotic behavior ($\beta_1=0.846$ fm^{-1} corresponds to the p-t separation energy in ^{4}He). A number of parameter sets $\{\alpha_i,\beta_i\}$ is now obtained corresponding to different models for the nucleon form factors $F_N(q^2)$, and to inclusion or noninclusion of meson exchange corrections. A more extensive report on these calculations will be given elsewhere.[31] In the present $(p,2p)$ calculations we only employed the set of parameters corresponding to a meson exchange corrected charge form factor, a standard dipole form for G_{E_p},[32] and a dispersion fit to G_{E_n}.[32] The quantities G_{E_p} and G_{E_n} are the electric form factor for the proton and neutron, respectively. The parameter set giving near perfect agreement with the electron charge form factor up to $q^2=60$ fm^{-2} is $\beta_i=[0.846+(i-1)1.42]$ fm^{-1}, and $\alpha_i=(4.84,\ -23.0,\ 47.3,\ -45.9,\ 16.8)$ fm$^{-1/2}$. In the fit, the last point measured by Arnold *et al.*[33] (at 64 fm^{-2}) was excluded, as all the predictions exceeded the bound on $|F_{\rm ch}(q^2)|$. Since it is highly unlikely that the simple cluster picture is reliable at such high momentum transfers, it is perfectly reasonable to omit this point. The wave

function fitted to the meson exchange corrected charge form factor as well as the wave function of Lim[26] are depicted in Fig. 10. Finally, it should be noticed that the wave functions calculated with and without meson exchange corrections differ much less than those in the calculations of Shepard *et al.*[29] In the latter case, the difference may have been enhanced by the constraints imposed on the charge form factor and therefore on the wave function.

VI. DISCUSSION

The results of the DWIA calculations for the energy sharing spectra are shown in Fig. 3 by the solid curves. It should be noted that the energy sharing spectra, as indicated above, reflect angular spreads different from those used to extract the coplanar symmetric angular distributions and those used to determine the energy dependence of the differential cross section corresponding to the exact quasifree scattering condition at symmetric angles. This was done to have consistency in the data for each of the three types of experiments presented here and to facilitate a comparison with previous results. There is reasonably good agreement with the shape of the energy sharing spectra although the calculations overestimate the zero recoil momentum point at 500 MeV. This overestimation of the differential cross section also becomes important towards lower incident proton energies as shown in Fig. 4 by the solid dots which give DWIA predictions as a function of energy at zero recoil momentum and symmetric angles. The agreement between the DWIA predictions and the data is best in the energy region where the *NN* total cross section has a minimum.

The results of the DWIA calculations for the coplanar symmetric angular distributions are shown in Fig. 5. Here, it should be noted that the calculations increasingly underestimate the data as the recoil momentum increases. This disagreement is one of the interesting results of this study. It was shown above that the use of the initial state approximation for the *p-p* scattering amplitude would only increase the discrepancy between theory and experiment. It should also be remarked that the overall agreement with the data is better for the coplanar symmetric angular distributions than for the energy sharing spectra. For the latter there is no consistent overestimation or underestimation of the differential cross sections by the DWIA predictions. The sensitivity with regard to the choice of the optical potentials was studied by varying the strengths of the various potential terms of the energy dependent average parameter set. As can be seen in Fig. 5, reducing the strengths of all spin-orbit potential terms to zero gives a minimum in the DWIA prediction at 400 MeV/c such that the calculation becomes a factor of 30 or more times smaller than experiment (dashed curve). This minimum in the DWIA prediction reflects the minimum in the ^{4}He charge form factor. Note that inclusion of spin-orbit potential terms leaves only a shoulder in the DWIA predictions and that the result is much closer to experiment. The sensitivity to the inclusion of spin-orbit terms in the optical potentials was suggested by the work of Chant *et al.*[34] These authors found that although the effect of including such terms is small ($<10\%$) for recoil momenta smaller than 150 MeV/c, the effect becomes increasingly more significant at larger recoil momenta. As expected, changes in the strength of the imaginary central potentials affect the magnitude of the DWIA cross sections. Changes in the other parameters, maintaining at the same time reasonable fits to the elastic scattering data, have much less influence on the DWIA predictions. This is demonstrated by comparing the DWIA predictions presented in an earlier paper[6] with those presented here for two different sets of optical model parameters, setting in both cases the spin-orbit potential term equal to zero. Applying a nonlocality correction to the optical model wave function as discussed by Perey and Buck[35] has no significant effect on the DWIA predictions ($<<10\%$ at the zero recoil momentum point and $\sim 10\%$ at 400 MeV/c).

The results of the DWIA calculations for the four point quasifree angular distributions at 250 and 500 MeV are shown in Fig. 7. Again, there is reasonably good agreement with the energy dependence of the data with the same overestimation of the magnitude of the cross sections. The quite unequal distribution in energies of the two observed protons make distortion effects important for the quasifree angular distributions.

The single particle wave functions which have been corrected for meson exchange current effects after fitting the ^{4}He charge form factor have less large momentum components than, for instance, the single particle wave function of Eckart form of Lim.[26] This is reflected in the DWIA predictions for the coplanar symmetric angular distributions at high recoil momenta (>400 MeV/c) for the Lim wave function giving results closer to experiment

[see Fig. 5 (500 MeV) dash-dot curve].

The disagreement between the DWIA predictions using the meson exchange current corrected wave function and the data at large recoil momenta may be due to the following. First, although great care was taken in obtaining an energy dependent average set of optical potential parameters, the intrinsic difficulty of representing proton-light-nucleus elastic scattering by an optical potential may reflect itself in inadequate distortions. Second, various rescattering and exchange terms may increase the differential cross section for large recoil momenta. An attempt to include such terms in a DWIA formulation is currently underway.[36] A comparison with ^{4}He$(e,e'p)^3$H data when these become available will give insight into the importance of rescattering effects. In Figs. 11(a) and (b), the content of various rescattering diagrams is schematically illustrated. The diagrams in Figs. 11(c) and (d) represent exchange processes characterized by the absence of an interaction between the two outgoing protons. Another correction to the DWIA stems from Pauli corrections to the free proton-proton scattering amplitude, which are thought to enhance the t matrix for large momentum transfers. However, Miller[37] found only a minor influence of the latter corrections for other nuclei. Furthermore, there exists the possibility that the triangular diagram illustrated in Fig. 11(e) gives a major contribution, as has been suggested for other processes such as (p,π) and (p,d), and in particular for p-d backward angle elastic scattering. Rescattering effects may also have a large influence on the analyzing powers of the ^{4}He$(\vec{p},2p)^3$H reaction, so that it is expected that the analyzing power data for the present reaction,[38] will provide important new information for testing multiple scattering effects. Finally, there exists the possibility that the proton-triton wave function which gives a good fit to the ^{4}He charge form factor, does not give an adequate description of the large momentum components in ^{4}He.

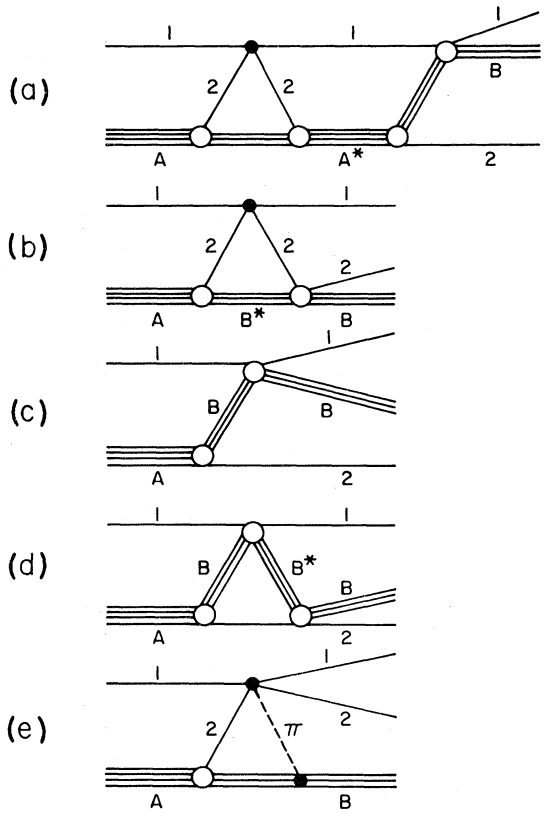

FIG. 11. Diagrams of rescattering and exchange effects not included in conventional DWIA calculations. Protons are indicated by 1, 2, and 3. The target nucleus (^{4}He) is indicated by A, while the recoil nucleus (^{3}He) is indicated by B. Asterisks indicate intermediate excited states.

ACKNOWLEDGMENTS

The authors would like to thank Dr. N. S. Chant for the use of his DWIA program and for many stimulating and clarifying discussions. This work was supported in part by the Natural Sciences and Engineering Research Council of Canada and by the U. S. National Science Foundation.

*Present address: Schlumberger Well Services, Houston, Texas 77023.

†Present address: NIKHEF-H, 1098 SJ Amsterdam, The Netherlands.

‡Present address: TRIUMF, Vancouver, British Columbia V6T 2A3, Canada.

[1]H. G. Pugh, P. G. Roos, A. A. Cowley, V. K. C. Chang, and R. Woody, Phys. Lett. 46B, 192 (1973).

[2]R. Frascaria, P. G. Roos, M. Morlet, N. Marty, A. Willis, V. Comparat, and N. Fujiwara, Phys. Rev. C 12, 243 (1975).

[3]H. Tyrén, S. Kullander, O. Sundberg, R. Ramachandran, P. Isacsson, and T. Berggren, Nucl. Phys. 79, 321 (1966).

[4]C. F. Perdrisat, L. W. Swenson, P. C. Gugelot, E. T. Boschitz, W. K. Roberts, J. C. Vincent, and J. R. Priest, Phys. Rev. 187, 1201 (1969).

[5]P. G. Roos, *Momentum Wave Functions—1976 (India-*

na University), Proceedings of the Workshop/Seminar on Momentum Wave Function Determination in Atomic, Molecular and Nuclear Systems, edited by D. W. Devins (AIP, New York, 1977), p. 32.

[6]M. B. Epstein, D. J. Margaziotis, J. Simone, D. K. Hasell, B. K. S. Koene, B. T. Murdoch, W. T. H. van Oers, J. M. Cameron, L. G. Greeniaus, G. A. Moss, J. G. Rogers, and A. W. Stetz, Phys. Rev. Lett. 44, 20 (1980).

[7]C. A. Goulding, B. T. Murdoch, M. S. de Jong, W. T. H. van Oers, and R. H. McCamis, Nucl. Instrum. Methods 148, 11 (1978).

[8]J. M. Cameron, P. Kitching, R. H. McCamis, C. A. Miller, G. A. Moss, J. G. Rogers, G. Roy, A. W. Stetz, C. A. Goulding, and W. T. H. van Oers, Nucl. Instrum. 143, 399 (1977).

[9]P. G. Roos, Phys. Rev. C 9, 2437 (1974).

[10]N. S. Chant, private communication.

[11]D. F. Jackson and T. Berggren, Nucl. Phys. 62, 353 (1965); D. F. Jackson, *ibid.* A257, 221 (1976).

[12]O. Chamberlain and M. O. Stern, Phys. Rev. 94, 666 (1954).

[13]T. R. Mongan, Phys. Rev. 184, 1888 (1969).

[14]R. A. Arndt, R. H. Hackman, and L. D. Roper, Phys. Rev. C 15, 1002 (1977); R. A. Arndt, private communication.

[15]J. Bystricky, F. Lehar, and Z. Janout, Centre D'Etudes Nucléaires de Saclay, Report CEA-N-1547(E), 1976 (unpublished).

[16]M. S. Kozodaev, N. M. Kulyukin, P. S. Sulyaev, A. I. Filippov, and Yu. A. Scherbakov, Zh. Eksp. Teor. Fiz. 38, 708 (1960).

[17]G. J. Igo, J. L. Friedes, H. Palevsky, R. Sutter, G. Bennet, W. D. Simpson, D. M. Corley, and R. L. Stearns, Nucl. Phys. B3, 181 (1967).

[18]M. A. Melkanoff, J. Raynal, and T. Sawada, University of California at Los Angeles, Report 66-10, 1966 (unpublished).

[19]W. T. H. van Oers, H. Haw, N. E. Davison, A. Ingemarsson, B. Fagerström, and G. Tibell, Phys. Rev. C 10, 307 (1974).

[20]S. W.-L. Leung and H. S. Sherif, Can. J. Phys. 56, 1116 (1978).

[21]H. O. Meyer, P. Schwandt, G. L. Moake, and P. P. Singh, Phys. Rev. C 23, 616 (1981).

[22]H. Collard, R. Hofstadter, E. B. Hughes, A. Johansson, M. R. Yearian, R. B. Day, and R. T. Wagner, Phys. Rev. 138, B57 (1965); J. S. McCarthy, I. Sick, and R. R. Whitney, Phys. Rev. C 15, 1396 (1977).

[23]B. T. Murdoch, D. K. Hasell, A. M. Sourkes, W. T. H. van Oers, and R. E. Brown, (unpublished); J. Birchall, W. T. H. van Oers, H. E. Conzett, P. von Rosen, R. M. Larimer, J. Watson, and R. E. Brown, *Polarization Phenomena in Nuclear Physics-1980* (5th Symp., Santa Fe) edited by G. G. Ohlsen, R. E. Brown, N. Jarmie, W. W. McNaughton, and G. M. Hale, (AIP, New York, 1981), p. 1263.

[24]B. S. Podmore and H. S. Sherif, *Few Body Problems in Nuclear and Particle Physics,* edited by R. J. Slobodian, B. Cujec, and K. Ramavataram (Les Presses de l"Université Laval, Quebec, 1975), p. 517; G. E. Thompson, M. B. Epstein, and T. Sawada, Nucl. Phys. A142, 571 (1970).

[25]I. Sick, J. S. McCarthy, and R. R. Whitney, Phys. Lett. 64B, 33 (1976).

[26]T. K. Lim, Phys. Lett. 44B, 341 (1973); and private communication.

[27]H. Leśniak, L. Leśniak, and A. Tekou, Nucl. Phys. A267, 503 (1976).

[28]J. M. Laget, J. F. Lecolley and F. Lefebvres, in *Proceedings of the Eighth International Conference on High Energy Physics and Nuclear Structure, Vancouver, 1979,* edited by D. F. Measday and A. W. Thomas (North-Holland, Amsterdam, 1980); and private communication.

[29]J. R. Shepard, E. Rost, and G. Smith, Phys. Lett. 89B, 13 (1979).

[30]M. Gari, H. Hyuga, and J. G. Zabolitzki, Nucl. Phys. A271, 365 (1976).

[31]J. M. Greben (unpublished).

[32]G. Höhler, E. Pietarinen, I. Sabba-Stefanescu, F. Borkowski, G. G. Simon, V. H. Walther, and R. D. Wendling, Nucl. Phys. B114, 505 (1976).

[33]R. G. Arnold, B. T. Chertok, S. Rock, W. P. Schütz, Z. M. Szalata, D. Day, J. S. McCarthy, F. Martin, B. A. Mecking, I. Sick, and G. Tamas, Phys. Rev. Lett. 40, 1429 (1978).

[34]N. S. Chant, P. Kitching, P. G. Roos, and L. Antonuk, Phys. Rev. Lett. 43, 495 (1979).

[35]F. G. Perey, Phys. Rev. 131, 745 (1963); F. G. Perey and B. Buck, Nucl. Phys. 32, 353 (1962).

[36]P. C. Tandy and R. M. Thaler, Bull. Am. Phys. Soc. 25, 519 (1980).

[37]C. A. Miller, in *Proceedings of the Ninth International Conference on Few-Body Problems, Eugene,* edited by F. S. Levin (North-Holland, Amsterdam, 1981) [special edition, Nucl. Phys. A353, 157 (1981)].

[38]M. B. Epstein, D. J. Margaziotis, R. Abegg, D. K. Hasell, W. T. H. van Oers, J. M. Cameron, G. A. Moss, L. G. Greeniaus, and A. W. Stetz, in *Polarization Phenomena in Nuclear Physics,-1980.* (5th Symp., Sante Fe), edited by G. G. Ohlsen, R. E. Brown, N. Jarmie, W. W. McNaughton, and G. M. Hale (AIP, New York, 1981), p. 1287.